The Company of Biologists

RESEARCH ARTICLE

The RNA ligase RNA terminal phosphate cyclase B regulates mRNA alternative splicing and is required for mouse oocyte development and maintenance

Hua Zhang[1,2,*], Jun-Chao Jiang[1,*], Yun-Wen Wu[1], Yuan-Song Yu[3], Hua-Nan Wang[2,‡], Nai-Zheng Ding[4,‡] and Heng-Yu Fan[1,‡]

ABSTRACT

Recent large-scale mRNA sequencing has shown that introns are retained in 5-10% of mRNA, and these events are named intron retention (IR). IR has been recognized as a key mechanism in the regulation of gene expression. However, the role of this mechanism in female reproduction in mammals remains unclear. RNA terminal phosphate cyclase B (RTCB) is a RNA ligase; we found that RTCB conditional knockout mice have premature ovarian failure and that RTCB plays a crucial role in follicular development. RTCB regulated the splicing of transcripts related to DNA methylation and DNA damage repair. In addition, it regulated the resumption of oocyte meiosis by affecting CDK1 activation. Moreover, the loss of RTCB suppressed zygotic genome activation (ZGA) and decreased translation at the global level. In addition, *Rtcb* deletion resulted in the accumulation of maternal mRNAs containing unspliced introns and in a decline in the overall level of transcripts. As a result, the *Rtcb*$^{-/-}$ females were sterile. Our study highlights the important role of RTCB-regulated noncanonical alternative splicing in female reproduction.

KEY WORDS: RNA processing, Transcriptome, Female fertility, Premature ovarian failure, Folliculogenesis, Oogenesis, Meiosis

INTRODUCTION

During the development of growing oocytes into fully grown oocytes, an increase in oocyte volume is coupled with active transcription events (Pangas and Rajkovic, 2006). Pre-mRNA is processed to remove introns and splice exons via alternative splicing (AS) (Darnell, 2013; Ding et al., 2014). Through AS, multiple transcripts and protein variants can be transcribed and translated from a single gene, which significantly enriches the diversity of transcriptomes and proteomes (Braunschweig et al., 2013; Stamm et al., 2005). Common AS events include intron retention (IR),

[1]MOE Key Laboratory for Biosystems Homeostasis and Protection and Innovation Center for Cell Signaling Network, Life Sciences Institute, Zhajiang University, Hangzhou 310058, China. [2]College of Animal Sciences, Zhejiang University, Hangzhou 310058, China. [3]Savaid Stomatology School, Hangzhou Medical College, Hangzhou 310053, China. [4]The Key Laboratory of Animal Resistant Biology of Shandong Province, College of Life Science, Shandong Normal University, Jinan 250014, China.
*These authors contributed equally to this work

‡Authors for correspondence (hyfan@zju.edu.cn; nzding@sdnu.edu.cn; hnwang@zju.edu.cn)

Y.-S.Y., 0000-0002-0382-8298; H.-N.W., 0000-0003-3162-2382; N.-Z.D., 0000-0001-9795-0616; H.-Y.F., 0000-0003-4544-4724

skipped exons (SE), mutually exclusive exons (MXE), and alternative 5′ and 3′ splice sites (A5SS and A3SS). Recent studies have shown that intron retention (IR) occurs in many mRNAs and is a frequent event in plants and humans (Ner-Gaon et al., 2004; Reddy et al., 2013). IR is recognized as a key mechanism in the regulation of gene expression. Specific transcripts with IR are expressed in specific cell types or situations, and therefore control developmental transitions or cellular stress responses (Boothby et al., 2013; Braunschweig et al., 2014; Shalgi et al., 2014; Wong et al., 2013).

During mRNA retained intron splicing, two half-molecules with 2′3′-cyclic phosphate and 5′-OH ends are considered unconventional products (Englert et al., 2012). There are two known pathways for rectifying these two ends. Classically, ligation occurs via a multienzyme pathway. Classical ligases catalyze the ligation of 5′-P and 3′-OH ends with the help of ATP and Mg^{2+} (Desai et al., 2013). Before sealing, 2′,3′-cyclic phosphate is hydrolyzed to 3′-OH by phosphodiesterase, and 5′-OH is phosphorylated by polynucleotide kinase to generate 5′-phosphate (5′-P). The second pathway depends on RTCB. The role of RTCB as an RNA ligase was recently confirmed. It directly ligates the 2′3′-cyclic phosphate and 5′-OH terminal half molecules (Desai et al., 2013; Popow et al., 2011; Tanaka et al., 2011a,b; Tanaka and Shuman, 2011). With the help of GTP and Mn^{2+} ions, RTCB can treat 2′3′-cyclic phosphate and 5′-OH ends in one step to form a phosphodiester bond (Chakravarty and Shuman, 2012; Chakravarty et al., 2012; Desai and Raines, 2012; Englert et al., 2012). RTCB plays a key role in tRNA maturation and splicing of *Xbp1* mRNA (Tanaka et al., 2011b), and can catalyze the reconnection of short 16S rRNA produced by stress (Maughan and Shuman, 2016). *Xbp1* is the only confirmed RTCB target mRNA (Lu et al., 2014). RTCB regulates the unfolded protein response (UPR) through the unconventional splicing of *Xbp1* mRNA in the cytoplasm (Shinya et al., 2011). RTCB also plays a key role in regulating tRNA splicing after intron removal (Tanaka et al., 2011b). According to a previous study, ∼5% of tRNA genes in mice contain introns (Wu and Hopper, 2014). tRNA introns are positioned downstream of the anticodon and are smaller than mRNA introns. After intron removal, these pre-tRNAs require ligation to form mature tRNAs. RTCB is responsible for catalyzing the ligation of these tRNAs.

Immature oocytes of mice are arrested at the germinal vesicle (GV) stage in growing ovarian follicles unless they are stimulated by a gonadotrophin signal or released from an inhibitory follicular environment. At this stage, GV oocytes can be classified based on their chromatin configuration in non-surrounded nucleolus (NSN) oocytes and surrounded nucleolus (SN) oocytes. NSN oocytes have low developmental competence and their chromatin does not form a Hoechst-positive rim around the nucleolus. In contrast, the

chromatin of SN oocytes forms a Hoechst-positive rim around the nucleolus, and transcription in SN oocytes is silenced (Tan et al., 2009). However, many of the synthesized mRNAs are stored in the ooplasm. The dormant mRNAs drive meiosis and early embryonic development. The key events of meiosis mainly include germinal vesicle breakdown (GVBD) and the following two consecutive M phases (MI and MII) (Jones, 2011).

Splicing factors in oocytes, such as SRSF3 and BCAS2, have been shown to play an important role in oocyte maturation and the maintenance of transcriptome integrity (Do et al., 2018; Zhang et al., 2022). Without RTCB, the lifespan of *Caenorhabditis elegans* decreases, germ cells fail to mature into oocytes, and the animals are rendered completely sterile (Kosmaczewski et al., 2014). We hypothesized that this new mechanism of rapid gene regulation via RTCB may also exist in mouse oocytes. To test this hypothesis, we specifically knocked out the *Rtcb* gene in oocytes as early as the primordial follicle stage using *Gdf9-Cre*. Our results show that RTCB is responsible for regulating mRNA splicing after intron removal during oocyte meiosis. The absence of RTCB resulted in the accumulation of a series of intron-containing transcripts, mainly including DNA methylation and DNA damage repair-related transcripts. As a result, the levels of these maternal proteins decreased. Follicular development, meiosis recovery and early embryonic development were impeded. In summary, our results confirm that RTCB-regulated alternative splicing plays an important role in female reproduction.

RESULTS

Rtcb is highly expressed in mouse oocytes and is indispensable for female fertility

First, we detected *Rtcb* expression in various tissues and organs by quantitative RT-PCR. The results showed that *Rtcb* was highly expressed in female germ cells (Fig. 1A). In addition, *Rtcb* mRNA levels remained relatively stable in oocytes and increased drastically after the two-cell stage (Fig. 1B). These results suggest that RTCB may play an important role in oocyte development and embryo preimplantation. Thereafter, we detected RTCB levels by western blotting (WB) during oocyte meiosis. The results showed that RTCB protein levels at the GVBD stage were higher than in the germinal vesicle (GV), MI and MII stages (Fig. 1C).

To study the *in vivo* function of RTCB in oocytes, we constructed oocyte-specific *Rtcb* knockout mice. By crossing *Rtcb*-floxed mice (*Rtcb*$^{fl/fl}$) with *Gdf9-Cre* transgenic mice, we deleted the *Rtcb* gene in oocytes as early as the primordial follicle stage (Fig. 1D). WB and immunofluorescence (IF) results revealed that RTCB protein was completely depleted in GV oocytes (Fig. 1E,G). IF results showed that RTCB was distributed in the nuclei and cytoplasm of the oocytes. In contrast, there was no RTCB signal in *Rtcb*-deleted oocytes (Fig. 1E). A subcellular fractionation assay of 293T cells also proved the nuclear and cytoplasmic localization of RTCB (Fig. 1F). This result is consistent with previous reports in HeLa cells (Jurkin et al., 2014). Thereafter, we conducted a fertility test for 7 months by mating *Rtcb*$^{fl/fl}$ female mice (hereafter referred to as wild type) and *Rtcb*$^{fl/fl}$;*Gdf9-Cre* female mice (hereafter referred to as *Rtcb*$^{oo−/−}$) with wild-type males. The *Rtcb*$^{oo−/−}$ female mice were completely sterile (Fig. 1H). These results demonstrate that RTCB in oocytes is required for female fertility in mice.

Rtcb deletion causes premature ovarian failure in mice older than 8 weeks

To study the effect of *Rtcb* deletion on follicle development in the ovary, we collected mouse ovaries at various stages and compared

their shapes and sizes. Compared with wild-type mice, the ovaries of 4-week-old *Rtcb*$^{oo−/−}$ mice (not stimulated by exogenous gonadotropins) were almost similar in size. However, in *Rtcb*$^{oo−/−}$ mice older than 6 weeks, the ovaries were significantly smaller than those of wild-type mice (Fig. 2A,B).

Subsequently, we investigated follicle development at various ages using Hematoxylin and Eosin staining, and immunohistochemistry (IHC). The ovaries of 4-week-old *Rtcb*$^{oo−/−}$ mice still contained many primordial, primary, secondary and antral follicles (Fig. 2C). Follicular counting results showed that the ovaries of 6-week-old *Rtcb*$^{oo−/−}$ mice (not stimulated by exogenous gonadotropins) contained similar numbers of primordial, primary and bilayer secondary follicles relative to wild-type mice, but fewer secondary and antral follicles with multilayer granulosa cells (Fig. 2D,H). Furthermore, fewer primordial, primary and secondary follicles remained in the ovaries of the 8-week-old mice (Fig. 2E and I). No follicles were found in the ovaries of 10-week-old or 7-month-old knockout mice (Fig. 2F,G).

To investigate why premature ovarian failure occurs, we examined the signal of phosphorylated H2AX (γH2AX, an unrepaired DNA lesion marker) in oocytes in ovarian sections. We found that, in 6-week-old *Rtcb*$^{oo−/−}$ mice, more than 50% of oocytes in secondary and antral follicles had obvious DNA damage signals (Fig. 2J,K). Moreover, TdT-mediated dUTP nick-end labeling (TUNEL) showed a higher proportion of apoptotic signals in the follicles of *Rtcb*$^{oo−/−}$ mice than in those of wild-type mice (Fig. 2L,M). In summary, these observations suggest that RTCB is essential for ovarian follicle development and that *Rtcb* deletion in oocytes leads to DNA damage and induced follicle atresia.

Rtcb deletion causes the accumulation of a series of maternal transcripts containing introns

Because fully grown GV oocytes were still present in the ovaries of 6-week-old *Rtcb*$^{oo−/−}$ mice, we analyzed the oocytes isolated from 6-week-old wild-type and knockout mice treated with pregnant mare serum gonadotropin (PMSG). The diameters of the *Rtcb*-null oocytes were significantly smaller than those of the wild-type oocytes (Fig. 3A,B). In addition, numerous brown cytoplasmic granules were detected in *Rtcb*-null oocytes (Fig. 3A). DAPI staining revealed that more than 80% of fully grown oocytes from 6-week-old wild-type mice had a surrounded nucleolus (SN) configuration. However, the proportion of SN configurations was only ~40% in the *Rtcb*-null oocytes (Fig. 3C,D). These results indicate that *Rtcb* deletion inhibited oocyte growth and nucleolar maturation.

To explore the effect of *Rtcb* deletion on maternal transcript levels, we collected fully grown GV oocytes from 6-week-old wild-type and knockout mice for RNA sequencing (RNA-seq) analyses. Gene expression levels were evaluated by fragments per kilobase of transcript per million mapped reads (FPKM). According to the RNA-seq results, we detected more genes with decreased mRNA copy numbers [1861 when fold change >2, false discovery rate (FDR) <0.05] than those with increased mRNA copy numbers (498 when fold change >2, FDR<0.05) (Fig. 3E). We performed gene ontology (GO) analysis on the decreased transcripts and found that they were mainly enriched in protein transport and DNA damage repair pathway (Fig. 3F), which may partially explain the phenotype of follicular atresia observed in 6-week-old *Rtcb*$^{oo−/−}$ mice. As RTCB mainly affects mRNA splicing, we tested the mRNA levels of the retained introns. We detected the level of transcripts containing intron retention (IR) using IRFinder
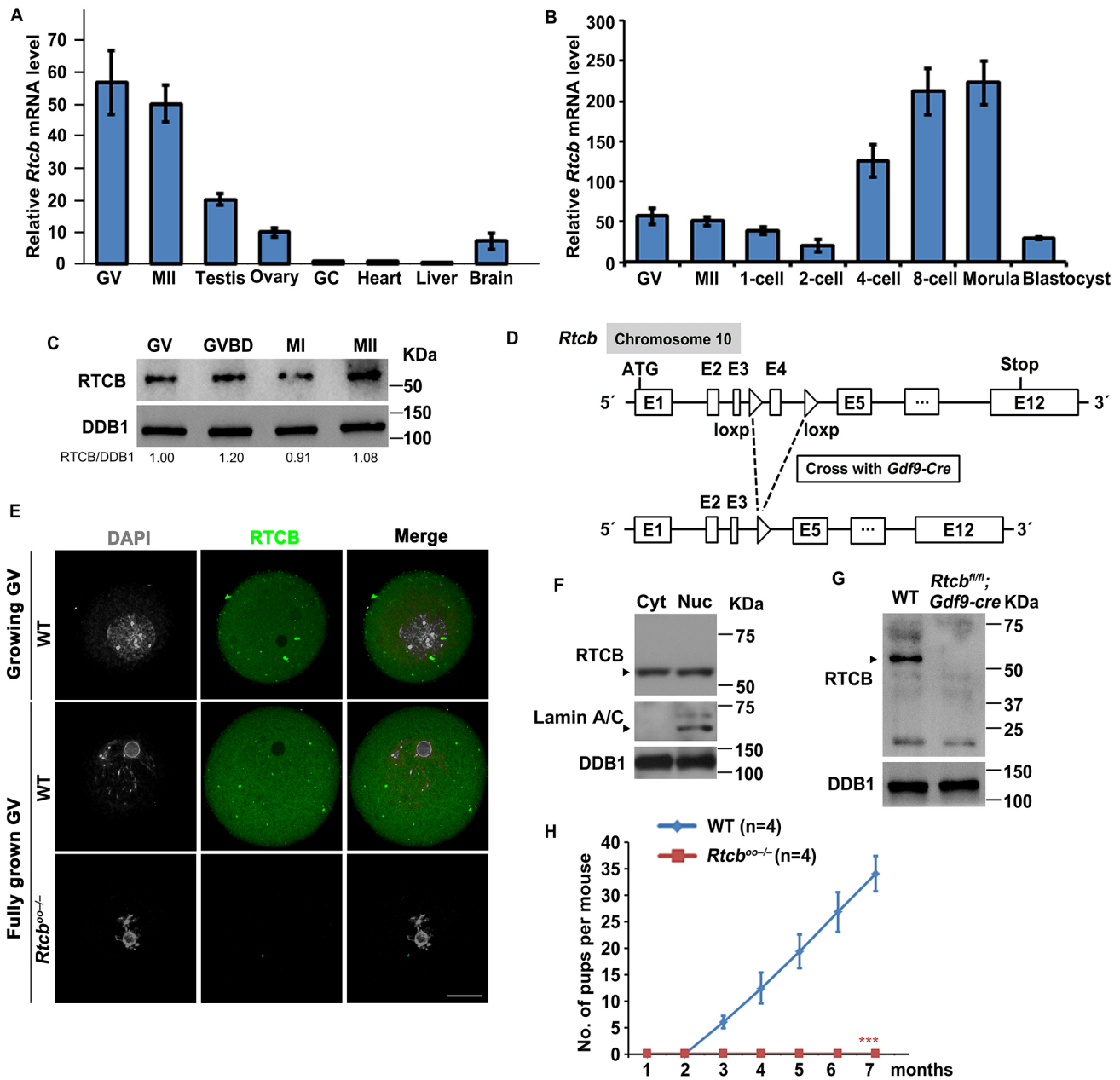
Fig. 1. The expression pattern of *Rtcb* mRNA and RTCB protein, and the phenotype of *Rtcb* knockout mice. (A,B) RT-qPCR results reveal the relative expression levels of mouse *Rtcb* mRNA in germinal vesicles (GV) and MII oocytes (A,B), in various tissues (A), and in preimplantation embryos (B). *n*=3 biological replicates. (C) Western blotting results show the expression levels of endogenous RTCB protein in GVs, in germinal vesicle breakdown (GVBD), and in MI and MII oocytes. DDB1 was used as a loading control. (D) Gene-targeting strategy for *Rtcb*-conditional knockout mouse. In *Rtcb* conditional knockout mice, the fourth exon of the *Rtcb* gene containing 100 bp is deleted, leading to premature translation termination. (E) Immunofluorescence (IF) results showing localization of endogenous RTCB in growing GV and fully grown GV oocytes from wild-type and *Rtcb^fl/fl^;Gdf9-Cre* female mice. Scale bar: 20 μm. (F) The nuclear and cytoplasmic separation samples of 293T cells were used for western blotting, and the results showed that RTCB protein existed in both cellular compartments. Lamin A/C was used as a nuclear marker, and DDB1 was used as a loading control. (G) Western blotting results show that RTCB protein is completely eliminated in *Rtcb^fl/fl^;Gdf9-Cre* female mice. The black arrowhead indicates the band corresponding to the RTCB protein. DDB1 was used as a loading control. (H) Cumulative number of pups per female mouse revealing the fertility of wild-type and *Rtcb^oo−/−^* female mice. *n*=4 females for each genotype. Data are mean±s.e.m. ***$P < 0.001$.

(Middleton et al., 2017). The IR ratio was calculated as the ratio of unspliced exon-intron junction reads to total junction reads (unspliced exon-intron and spliced exon-exon). The IR change was calculated from the IR ratio of knockout samples minus that of wild-type samples (Fig. 3G). According to IRFinder analysis, we detected many retained introns (Fig. 3I and Table S1). When IR change>0.1 and $P < 0.1$, 91 transcripts containing IR were detected

(Fig. 3H and Table S2). In addition, we used rMATS software to analyze other AS events (Shen et al., 2014). In addition to IR, many other AS events underwent significant changes because of *Rtcb* deletion (Fig. 3J and Table S3). GO enrichment analysis of different splicing events showed that RNA splicing was the most affected (Fig. S1). Based on these results, we conclude that RTCB plays a crucial role in RNA splicing in GV oocytes.
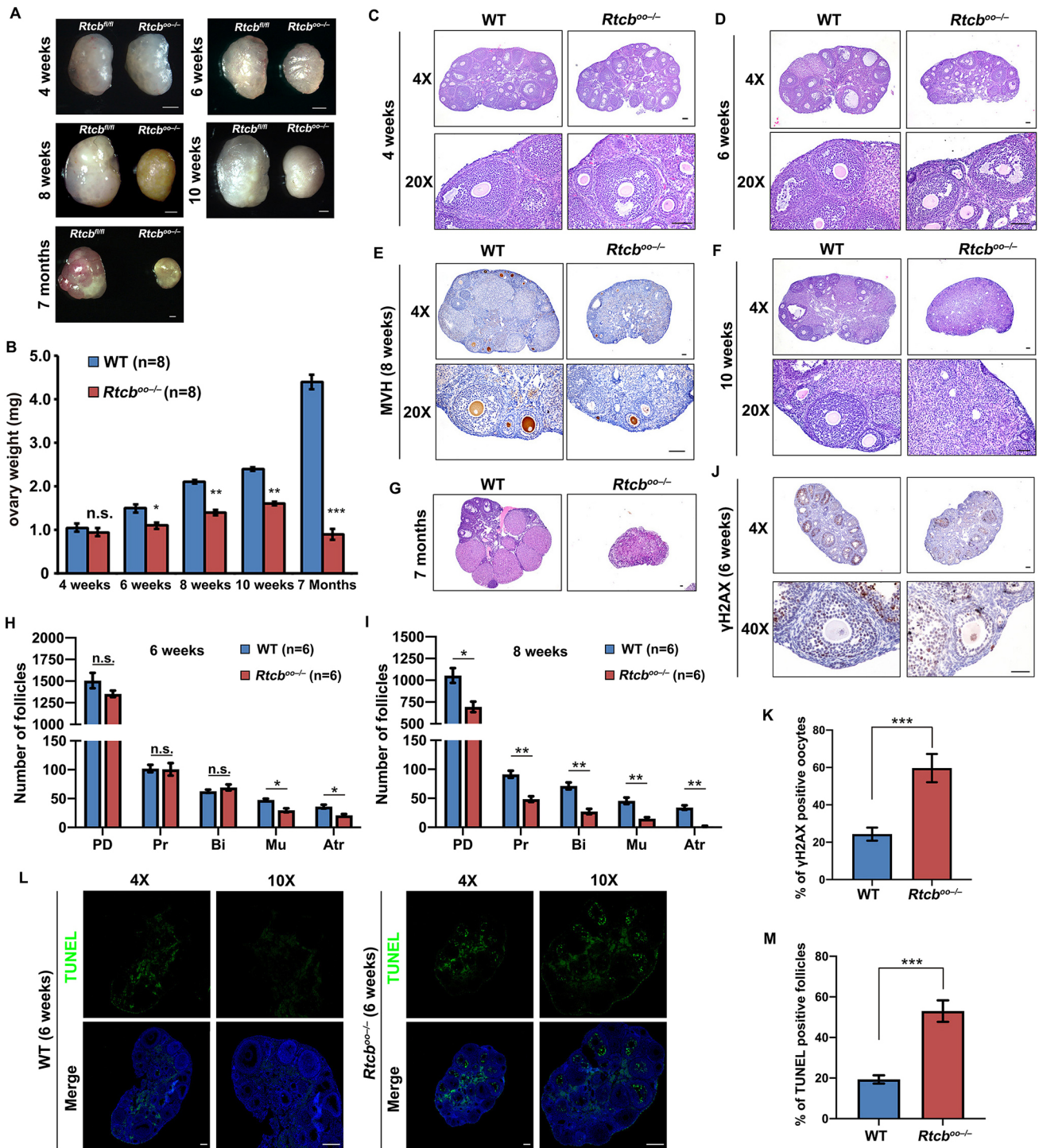
Fig. 2. *Rtcb* deletion in oocytes results in follicular development defects. (A) Representative ovaries from week 4, week 6, week 8 and week 10, and 7-month-old mice with indicated genotypes. Scale bars: 500 μm. (B) The ovary weight of wild-type and *Rtcb*^oo−/− mice, as in A. Data are mean±s.e.m. *P<0.05, **P<0.01, ***P<0.001. n.s. indicates a non-significant result. (C,D) Hematoxylin and Eosin staining results revealing ovarian histology of 4- and 6-week-old mice with indicated genotypes. Scale bars: 100 μm. (E) Immunohistochemistry staining of mouse VASA homolog (MVH, a germ cell marker) in the ovaries of 8-week-old mice with indicated genotypes. Scale bars: 100 μm. (F,G) Hematoxylin and Eosin staining results reveal ovarian histology of 10-week-old and 7-month-old mice with indicated genotypes. Scale bars: 100 μm. (H) The number of follicles at indicated stages in the ovaries of 6-week-old wild-type and *Rtcb*^fl/fl^*;Gdf9-Cre* female mice. Follicles were counted on serial ovarian sections after Hematoxylin and Eosin staining. Data are mean±s.e.m. *P<0.05, n.s. indicates a non-significant result. PD, primordial follicles; Pr, primary follicles; Bi, secondary follicles with two layers of granulosa cells; Mu, secondary follicles with multiple layers of granulosa cells; Atr, antral follicles. (I) The number of follicles at indicated stages in the ovaries of 8-week-old wild-type and *Rtcb*^fl/fl^*;Gdf9-Cre* female mice. Follicles were counted on serial ovarian sections after Hematoxylin and Eosin staining. Data are mean±s.e.m. *P<0.05, **P<0.01. n.s. indicates a non-significant result. (J) Immunohistochemistry staining of phosphorylated H2AX (γH2AX, an unrepaired DNA lesions marker) in the ovaries of 6-week-old mice with indicated genotypes. Scale bars: 100 μm. (K) Quantification of γH2AX-positive oocytes in the ovaries of 6-week-old mice with indicated genotypes. Data are mean±s.e.m. ***P<0.001. (L) Immunofluorescence (IF) staining of TUNEL in the ovaries of 6-week-old mice with indicated genotypes. Scale bars: 100 μm. (M) Quantification of TUNEL-positive follicles in the ovaries of 6-week-old mice with indicated genotypes. Data are mean±s.e.m. ***P<0.001.
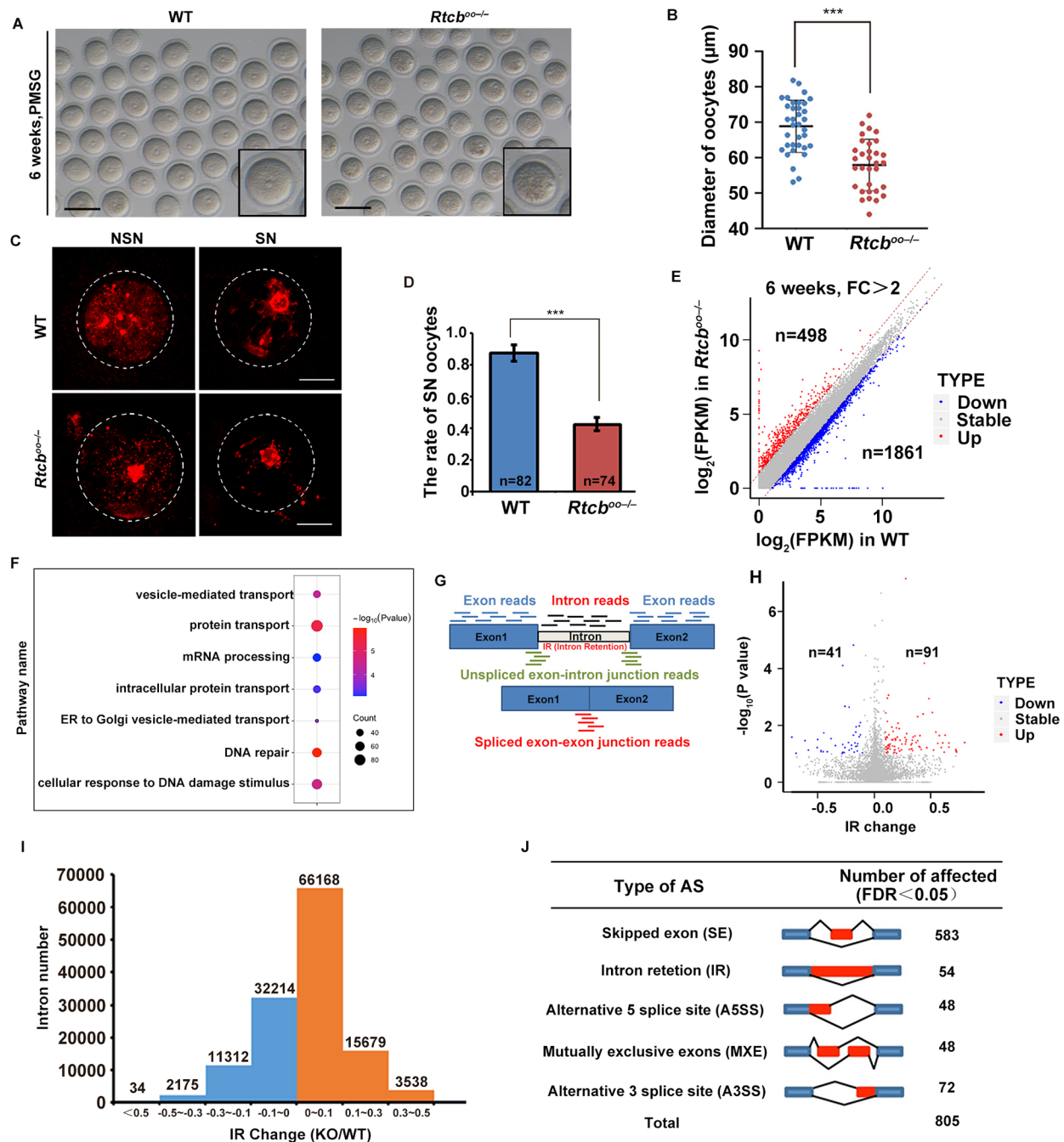
Fig. 3. Transcriptome and intron retention changes in *Rtcb*-deleted fully grown oocytes. (A) Representative images of germinal vesicle (GV) stage oocytes derived from 6-week-old wild-type and *Rtcb*[oo−/−] females. *n*=5 mice for each genotype. Scale bars: 100 μm. (B) Quantitative statistical results of oocyte diameter length derived from wild-type and *Rtcb*[oo−/−] females in A. Data are mean±s.e.m. ***P<0.001. (C) DAPI staining showed the non-surrounded nucleolus (NSN) and surrounded nucleolus (SN) chromatin configurations in wild-type and *Rtcb*[oo−/−] oocytes. Scale bars: 10 μm. (D) The rate of SNs in GV oocytes in A. Data are mean±s.e.m. ***P<0.001. (E) Scatter plot comparing transcripts between wild-type and *Rtcb*[oo−/−] fully grown GV oocytes. Transcripts increased or decreased more than twofold in *Rtcb*[oo−/−] oocyte samples are highlighted with blue or red, respectively. (F) Gene ontology analysis of downregulated genes in *Rtcb*[oo−/−] fully grown GV oocytes. (G) Schematic diagram revealing distribution of sequence reads for IR. The IR ratio is calculated from the ratio of unspliced exon-intron junction reads to total junction reads (unspliced exon-intron and spliced exon-exon). (H) Scatter plot showing the number of transcripts whose IR change increased or decreased more than 0.1 with *P*<0.1. IR change is calculated by subtracting the IR value of wild-type oocyte samples from the IR value of *Rtcb*[oo−/−] oocyte samples. (I) The intron number corresponding to different IR ratio changes (knockout/WT). (J) The number of transcripts corresponding to various alternative splicing (AS) events detected by rMATS. FDR<0.05.

The lack of maternal RTCB proteins causes epigenetic changes in oocytes

Based on previous results, we conclude that *Rtcb* deletion leads to IR accumulation and decreases many maternal mRNA levels. To determine whether IR accumulation can lead to changes in mRNA levels, we analyzed 91 transcripts with significant IR changes (eight transcripts from two identical genes were merged). The results showed that the expression levels of most transcripts decreased
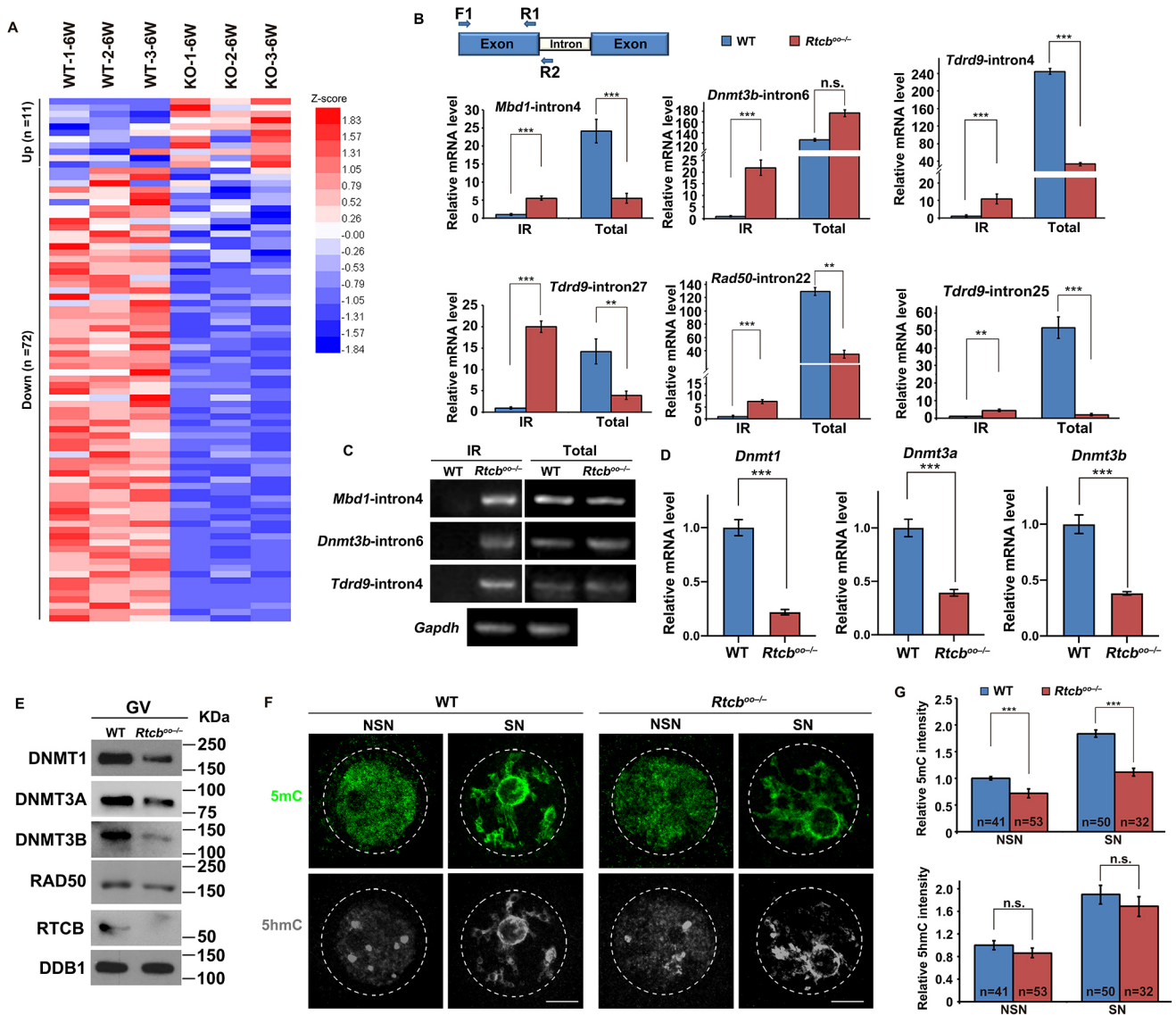
Fig. 4. The effect of maternal RTCB deficiency on epigenetic regulation. (A) Heatmap of genes showing the change of these transcripts having a significant IR accumulation due to *Rtcb* deletion. The value in the figure represents the relative level of mRNA. More details are included in Table S2. (B) IR analysis of several transcripts using RT-qPCR. Forward primer 1 and reverse primer 1 are designed to detect the level of the total transcripts. Forward primer 1 and reverse primer 2 are designed to detect the level of transcripts containing intron retention. Data are mean±s.e.m. **P<0.01, ***P<0.001. n.s. indicates a non-significant result. (C) PCR analysis results of some transcripts in A. *Gapdh* was used as a loading control. (D) Changes of relative mRNA copy numbers of indicated transcripts in wild-type and *Rtcb*oo−/− fully grown oocytes. Data are mean±s.e.m. ***P<0.001. (E) Western blotting results showing the expression levels of DNMT1, DNMT3A, DNMT3B and RAD50 proteins in wild-type and *Rtcb*oo−/− oocytes. DDB1 was used as a loading control. Total proteins from 200 oocytes were loaded into each lane. (F) Immunofluorescent staining showing the level of 5-hydroxymethylcytosine (5hmC) and 5-methylcytosine (5mC) derived from wild-type and *Rtcb*-deleted oocytes in the non-surrounded nucleolus (NSN) and surrounded nucleolus (SN) stages. Scale bars: 20 μm. (G) Quantification of 5hmC and 5mC in C. Data are mean±s.e.m. ***P<0.01. n.s. indicates a non-significant result.

(Fig. 4A). Thereafter, we confirmed the IR of these transcripts by RT-qPCR. MBD1 (methyl-CpG binding domain protein 1), also known as CXXC3, plays an important role in DNA methylation (Jørgensen et al., 2004). DNMT3B (DNA methyltransferase 3β) is responsible for establishing DNA methylation (Chen et al., 2004). TDRD9 is an ATP-binding RNA helicase required for spermatogenesis (Guijo et al., 2018). RAD50 is a component of the MRN complex and plays a vital role in double-strand break (DSB) repair (Iijima et al., 2008; Syed and Tainer, 2018). RT-qPCR results showed that IR occurred in these transcripts and that all three introns of *Tdrd9* were retained. In addition, the levels of most transcripts decreased (Fig. 4B). Visual assessment of RT-PCR products through agarose gel electrophoresis showed that IR events occur

in these transcripts after RTCB depletion. (Fig. 4C). The RNA-seq results also showed a decrease in *Dnmt1*, *Dnmt3a* and *Dnmt3b* mRNA levels (Fig. 4D).

As *Rtcb* deletion resulted in the IR of DNA methylation-related mRNAs, such as *Dnmt3b* and *Mbd1*, we detected changes in the levels of these related proteins. The results showed that the levels of DNMT1, DNMT3A, DNMT3B and RAD50 were decreased (Fig. 4E). In addition, IF staining showed that the levels of 5-methylcytosine (5mC) rather than 5-hydroxymethylcytosine (5hmC) in *Rtcb*oo−/− SN oocytes were significantly downregulated compared with those in wild-type oocytes (Fig. 4F,G).

These results demonstrate that by affecting RNA splicing, RTCB regulates the transcription of other maternal epigenetic regulators

6
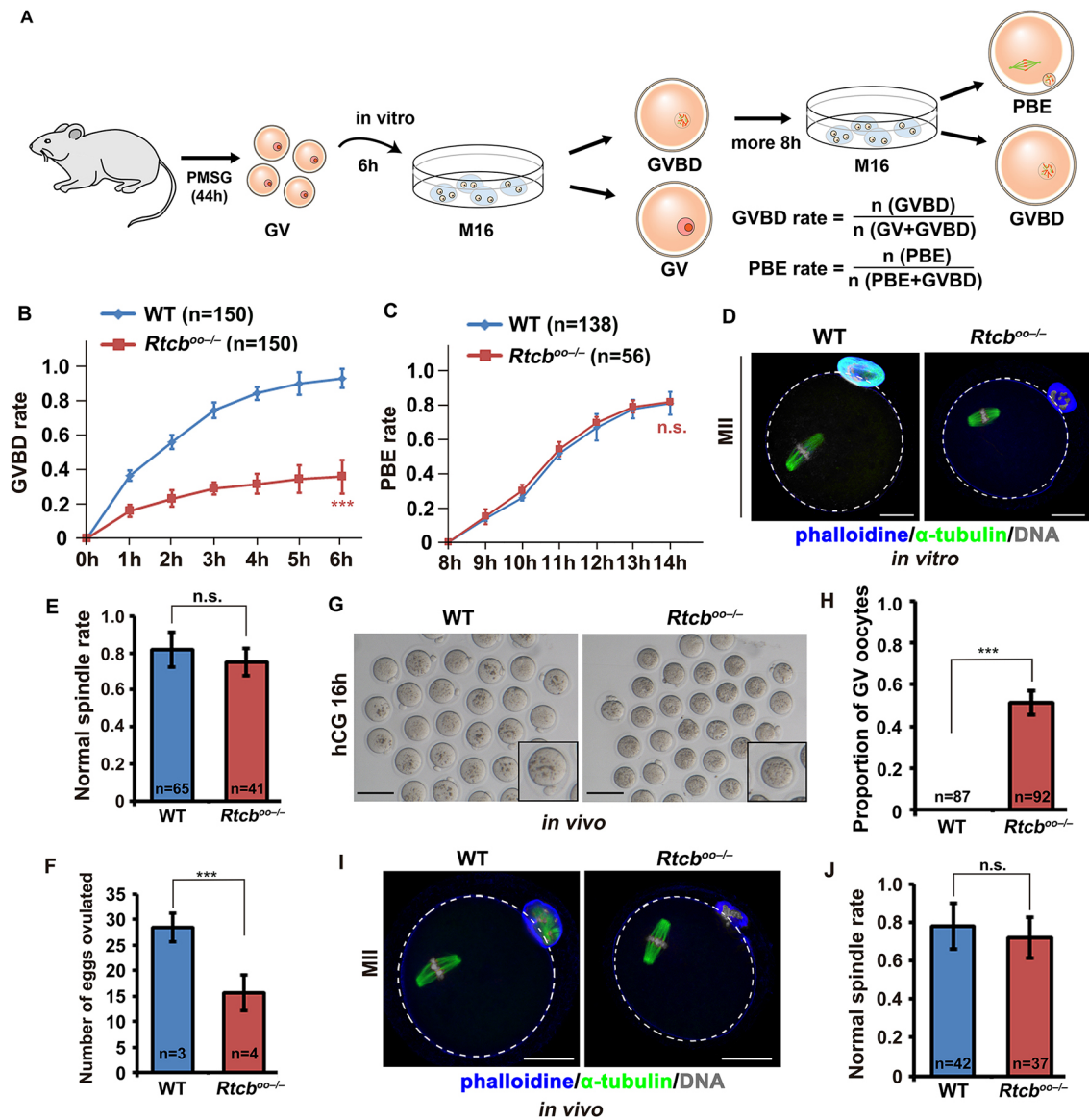
Fig. 5. The effect of *Rtcb* deletion on oocyte meiosis resumption. (A) Schematic diagram of oocyte culture *in vitro* and calculation method of oocyte germinal vesicle breakdown (GVBD) and polar body emission (PBE) rate. (B) Comparison of germinal vesicle breakdown (GVBD) kinetics in cultured wild-type and *Rtcb*$^{oo-/-}$ oocytes. (C) Kinetics of polar body emission (PBE). When oocytes undergo GVBD within 6 h, they are selected for further culture. Data are mean±s.e.m. ***P<0.01. n.s. indicates a non-significant result. (D) Immunofluorescence (IF) results show spindle assembly and chromosome alignment in wild-type and *Rtcb*$^{oo-/-}$ oocytes. Scale bars: 20 μm. (E) Rates of oocytes revealing normal spindle morphology as in C. Data are mean±s.e.m. n.s. indicates a non-significant result. (F) The number of ovulated eggs in E. Data are mean±s.e.m. ***P<0.01. (G) Representative images of MII oocytes derived from 6-week-old wild-type and *Rtcb*$^{oo-/-}$ females treated with hCG for 16 h. *n*=5 mice for each genotype. Scale bars: 100 μm. (H) The proportion of GV oocytes derived from ovulated oocytes in G. (I) IF results showing spindle assembly and chromosome alignment in ovulated MII oocytes derived from wild-type and *Rtcb*$^{oo-/-}$ females. Scale bars: 20 μm. (J) Rates of oocytes revealing normal spindle morphology as in H. Data are mean±s.e.m. ***P<0.01. n.s. indicates a non-significant result.

and DSB repair factors during oocyte growth, and renders developmental competence to oocytes. When *Rtcb* is deleted, IR occurs in many DNA methylation- and DNA damage repair-related transcripts, and the total levels of these transcripts are downregulated.

Rtcb-null oocytes fail to accomplish meiosis resumption

As *Rtcb* deletion led to the accumulation of introns among maternal transcripts, we then investigated whether these retained introns affected the normal progression of oocyte meiosis by measuring the development rate at different time points in oocytes cultured *in vitro* (Fig. 5A). *In vitro* culture results showed that *Rtcb* deletion

significantly downregulated the GVBD rate (Fig. 5B). However, *Rtcb*-null oocytes that were able to resume meiosis showed polar body emission (PBE) rates comparable with those of the wild-type oocytes (Fig. 5C). IF results showed that the absence of RTCB had a minor effect on chromosome alignment and spindle organization in MII oocytes (Fig. 5D,E). We also obtained oocytes from oviducts 16 h after human chorionic gonadotropin (hCG) injection. The *Rtcb*-null oocytes could be ovulated after hCG injection; however, the number of ovulated oocytes from *Rtcb*$^{oo-/-}$ mice was only half that in the control mice (Fig. 5F). In addition, half of the ovulated oocytes were arrested at the germinal vesicle (GV) stage (Fig. 5G,H). Similar to the *in vitro* results, these ovulated *Rtcb*-null
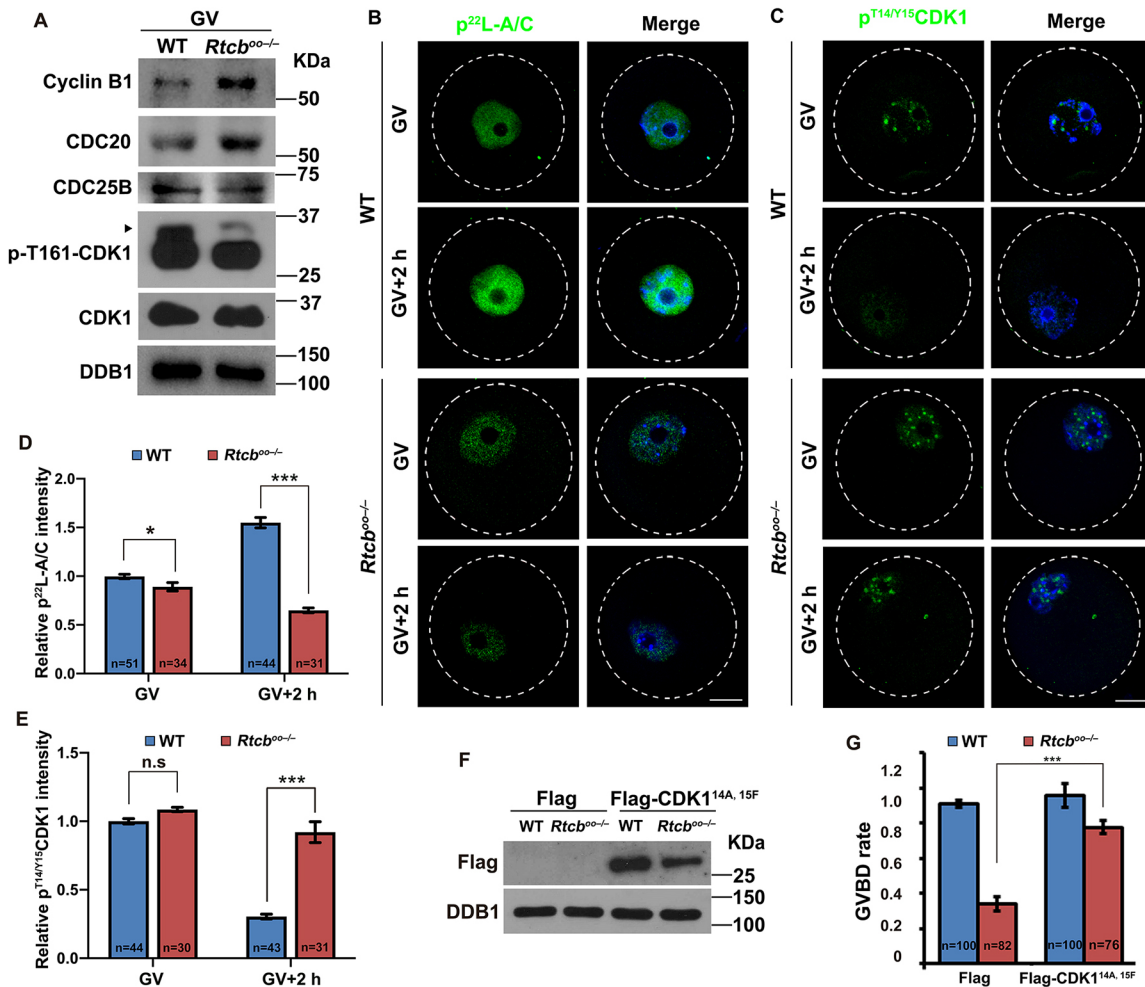
Fig. 6. *Rtcb*-null oocytes with inhibitory CDK1 lack phosphorylated lamin A/C and fail to GVBD. (A) Western blotting results showing the level of indicated proteins in GV oocytes derived from wild-type and *Rtcb*$^{oo-/-}$ females. DDB1 was used as a loading control. Total proteins from 200 oocytes were loaded in each lane. (B,C) Immunofluorescent (IF) staining showing the level of p$^{T14/Y15}$CDK1 and p^{S22}lamin A/C in oocytes at GV and GV+2 h stages derived from wild-type and *Rtcb*-deleted mice. Scale bars: 20 μm. (D,E) Quantification of p$^{T14/Y15}$CDK1 and p^{S22}lamin A/C in B and C. Data are mean±s.e.m. *$P<0.05$, ***$P<0.001$. n.s. indicates a non-significant result. (F) Western blotting (WB) results show the level of Flag-CDK1^{T14A,Y15F} in GV oocytes derived from wild-type and *Rtcb*$^{oo-/-}$ females. The FLAG lines were microinjected with the mRNA products of an empty vector with a FLAG tag. DDB1 was used as a loading control. Total proteins from 100 oocytes were loaded in each lane. (G) GVBD rates of cultured wild-type and *Rtcb*$^{oo-/-}$ oocytes with or without CDK1^{T14A,Y15F} expression in M16 medium. Data are mean±s.e.m. ***$P<0.001$. n.s. indicates a non-significant result.

MII oocytes showed normal chromosomal alignment and spindle organization (Fig. 5I,J). In summary, these results suggest that a lack of RTCB mainly affects meiosis resumption and has a minor effect on the subsequent PBE process.

CDK1 activity is reduced in *Rtcb*-null oocytes and lamin A/C cannot be phosphorylated

We examined the effects of *Rtcb* deletion on the levels of meiotic resumption-related proteins. Cyclin B1 is a key cell cycle-regulating protein that promotes G2/M transition (Adhikari and Liu, 2014). CDC20 is a positive regulator of the anaphase-promoting complex (APC) (Sudakin et al., 2001). However, WB results revealed that the levels of cyclin B1 and CDC20 proteins increased because of *Rtcb* deletion. Resumption of meiosis requires activation of cyclin-dependent kinase 1(CDK1), and phosphatase cell division cycle 25 B (CDC25B) is an activator of cyclin-dependent kinases (Lincoln et al., 2002). The dephosphorylation of threonine 14 and tyrosine 15 of CDK1 by CDC25 phosphatases is a key step in the activation of CDK1-cyclin B protein kinase (Morgan, 1995). We found that the

levels of CDC25B and p-T161-CDK1 proteins were lower than those in the wild-type oocytes (Fig. 6A).

Phosphorylated lamin A/C (p^{S22}lamin A/C) is a direct substrate of active phosphorylated CDK1 (Heald and McKeon, 1990). Therefore, we examined changes in the inhibitory phosphorylation of CDK1 (p$^{T14/Y15}$CDK1) and p^{S22}lamin A/C. In wild-type GV oocytes, p$^{T14/Y15}$CDK1 levels decreased and p^{S22}lamin A/C levels increased when GVBD was about to occur (GV oocytes cultured for 2 h). However, in the *Rtcb*-null oocytes cultured in the same manner, the p$^{T14/Y15}$CDK1 levels remained high and lamin A/C was not successfully phosphorylated (Fig. 6B-E). This observation indicates that the decline in CDC25B leads to the persistent phosphorylation of CDK1 on threonine 14 and tyrosine 15, and the failure of CDK1 phosphorylation on threonine 161. Consequently, lamin phosphorylation and GVBD failed to occur.

To further test our hypothesis, we overexpressed continuously activated CDK1 (CDK1^{T14A,Y15F}) in wild-type and *Rtcb*-null oocytes at the germinal vesicle (GV) stage (Fig. 6F). The GVBD rate of *Rtcb*-null oocytes overexpressing CDK1^{T14A,Y15F} was ~70%
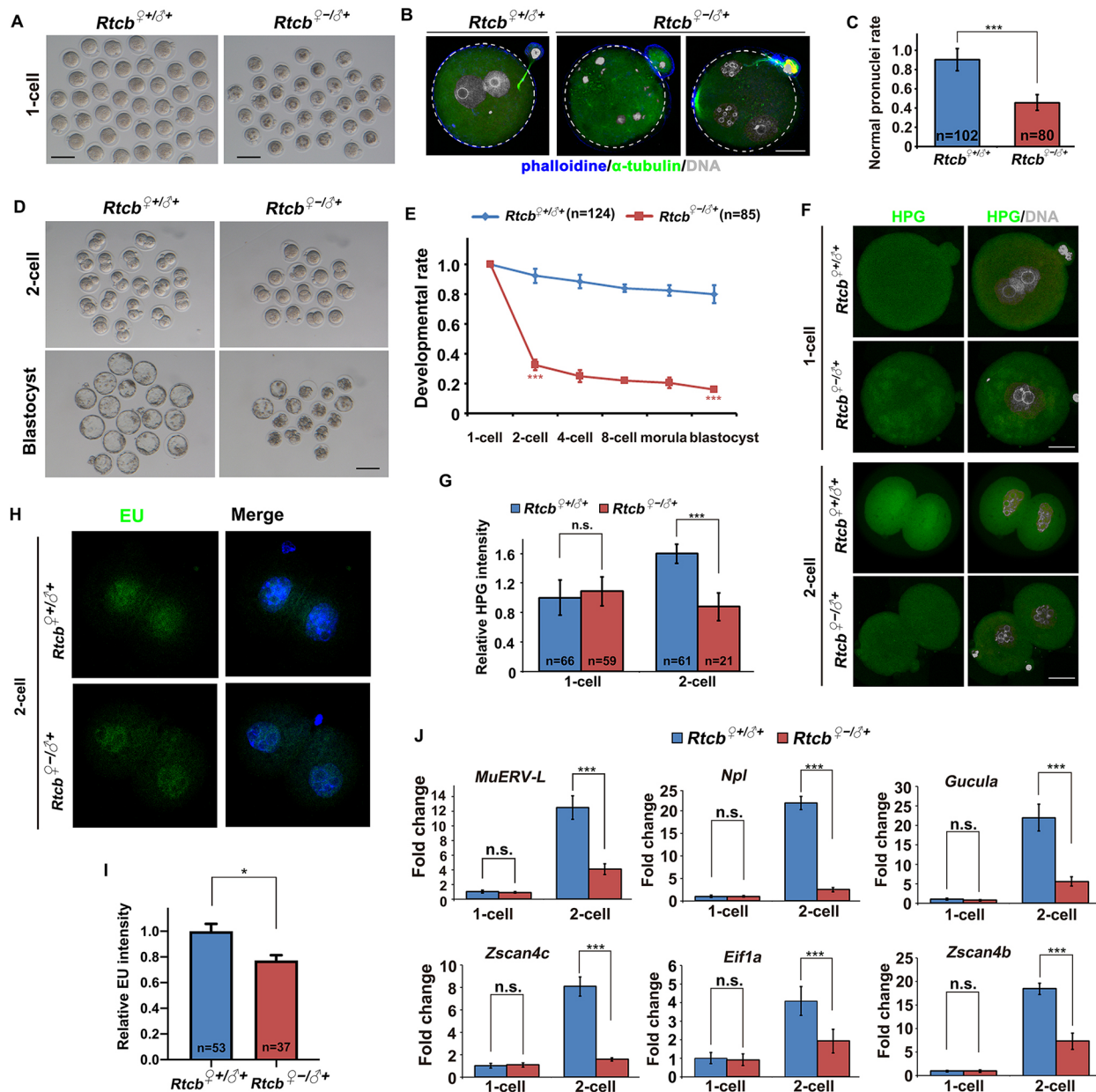
Fig. 7. The lack of maternal RTCB protein causes defects in early embryonic development. (A) Representative images of one-cell stage embryos derived from wild-type and $Rtcb^{oo-/-}$ females. n=5 mice for each genotype. Scale bars: 100 µm. (B) Immunofluorescence (IF) results showing the pronucleus formation of $Rtcb^{♀+/♂+}$ and $Rtcb^{♀-/♂+}$ zygotes. Scale bar: 20 µm. (C) The rate of one cell having normal pronuclei in A. (D) Representative images of two-cell stage embryos and a blastocyst derived from wild-type and $Rtcb^{oo-/-}$ females. n=5 mice for each genotype. Scale bar: 100 µm. (E) Developmental rates of maternal $Rtcb$-deleted embryos at the time when wild-type embryos reached corresponding stages. Data are mean±s.e.m. ***P<0.001. (F) L-homopropargylglycine (HPG) staining results show protein synthesis activity at the one-cell and two-cell stages in $Rtcb^{♀+/♂+}$ and $Rtcb^{♀-/♂+}$ embryos. Before staining, these embryos were incubated in medium containing 50 µM HPG for 1 h. Scale bars: 20 µm. (G) Quantification of HPG signal intensity in F. Data are mean±s.e.m. ***P<0.001. n.s. indicates a non-significant result. (H) IF of 5-ethynyl uridine (EU) fluorescence showing RNA transcription in $Rtcb^{♀+/♂+}$ and $Rtcb^{♀-/♂+}$ two-cell stage embryos. Scale bar: 20 µm. (I) Quantification of EU signal intensity in H. Data are mean±s.e.m. *P<0.05. (J) RT-qPCR results showing the expression level of zygotic genome activation (ZGA)-related genes at the one- and two-cell stages in $Rtcb^{♀+/♂+}$ and $Rtcb^{♀-/♂+}$ embryos. Data are mean±s.e.m. ***P<0.001. n.s. indicates a non-significant result.

AQ8

(Fig. 6G). This result indicates that RTCB plays an important role in maintaining the levels of activated CDK1 proteins.

Maternal RTCB protein is essential for zygotic genome activation and early embryonic development

Thereafter, we superovulated 6-week-old wild-type and $Rtcb^{oo-/-}$ females and mated them with wild-type males. The diameters of the zygotes obtained from $Rtcb^{oo-/-}$ mice were significantly smaller than those of the wild-type mice, and brown cytoplasmic granules aggregated in maternal $Rtcb$-deleted (hereafter $Rtcb^{♀-/♂+}$) zygotes (Fig. 7A). IF results showed many abnormal or multiple pronuclei in $Rtcb^{♀-/♂+}$ zygotes (Fig. 7B). The proportion of $Rtcb^{♀-/♂+}$ zygotes containing normal pronuclei was significantly lower than that of $Rtcb^{♀+/♂+}$ zygotes (Fig. 7C). Subsequently, zygotes were cultured in
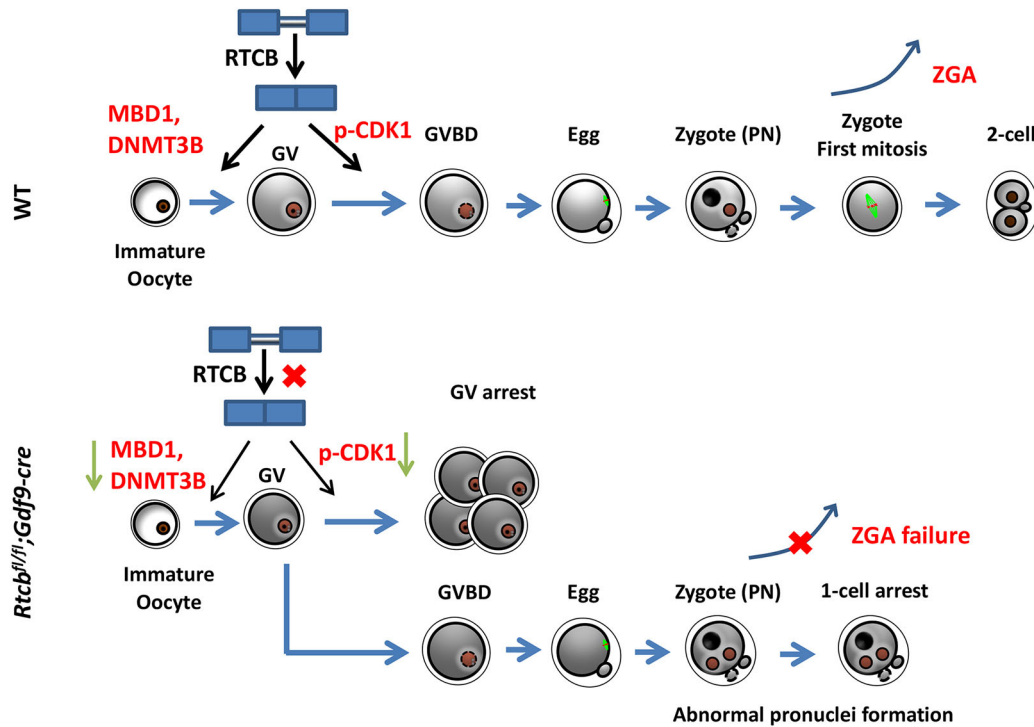
Fig. 8. Model representing the role of RTCB-regulated alternative splicing in meiosis and early embryonic development. RTCB-regulated RNA splicing is essential for oocyte growth and embryo development (wild type, top). *Rtcb* deletion in oocytes (bottom) resulted in intron retention (IR) of many transcripts such as *Mbd1*, *Rad50* and *Dnmt3b*. IR accumulation led to the downregulation of corresponding protein expression and insufficient oocyte growth. In addition, by influencing the protein level of p-CDK1 and p-Lamin A/C, the meiosis recovery of most oocytes was blocked. Even if a few oocytes could complete the meiosis recovery, the previous insufficient growth and abnormal pronucleus formed during the fertilization process led to the failure of ZGA. As a result, most zygotes were arrested at the one-cell stage.

KSOM medium. Although most $Rtcb^{♀+/♂+}$ zygotes developed to the two-cell stage, ~70% of $Rtcb^{♀−/♂+}$ zygotes underwent cell cycle arrest at the one-cell stage. However, fewer than 20% of $Rtcb^{♀−/♂+}$ zygotes developed into blastocysts (Fig. 7D,E). These results indicate that maternal RTCB is important for early embryonic development. However, as *Rtcb*-null oocytes suffer from maturation obstacles, subsequent defects in early embryonic development may be secondary effects caused by defective oocytes.

To detect the global translation level, we incubated wild-type and $Rtcb^{♀−/♂+}$ embryos at the one- and two-cell stages with L-homopropargylglycine (HPG), an analog of methionine that can be examined using the Click-iT cell reaction kit (Life Technologies) (Zhang et al., 2019). At the one-cell stage, the level of the HPG signal was not significantly different between the wild-type and $Rtcb^{♀−/♂+}$ zygotes. However, $Rtcb^{♀−/♂+}$ two-cell embryos showed weaker HPG signals than the wild-type embryos (Fig. 7F,G).

To evaluate whether zygotic genome activation (ZGA) was suppressed in arrested $Rtcb^{♀−/♂+}$ embryos, we labeled newly synthesized RNAs with 5-ethynyl uridine (EU) added to the culture medium 2 h before fixation of the one-cell stage. EU signals were lower in $Rtcb^{♀−/♂+}$ embryos than in $Rtcb^{♀+/♂+}$ (Fig. 7H,I). To confirm that ZGA was suppressed in the arrested $Rtcb^{♀−/♂+}$ embryos, we examined the expression of six ZGA-related transcripts [*MuERV-L* (*Erv4*), *Npl*, *Gucula* (xxxxx), *Zscan4c*, *Eif1a* and *Zscan4b*] using quantitative RT-PCR at the one- and two-cell stages. The levels of these transcripts should increase during ZGA in $Rtcb^{♀+/♂+}$ embryos; however, their transcriptional activation was significantly suppressed in $Rtcb^{♀−/♂+}$ embryos (Fig. 7J).

In summary, because of the lack of RTCB protein in oocytes, ZGA is suppressed and the global protein translation level is downregulated, leading to embryonic development arrest. These results indicate that maternal RTCB proteins are important for ZGA and early embryonic development.

DISCUSSION

Among the various AS events, intron retention has been frequently reported in various species. mRNA isoforms that contain introns are not useless. They are temporarily preserved in the cytoplasm and then spliced to synthesize functional proteins during developmental transitions or the cellular stress response. The ligation of these RNAs after intron removal is regulated by the RNA ligase RTCB. According to previous studies, IR occurs in many physiological processes, including the unfolded protein response, tRNA and 16S rRNA splicing (Maughan and Shuman, 2016; Shinya et al., 2011; Tanaka et al., 2011b). However, the role of IR in oocyte meiosis is still vague.

Many maternal mRNAs and proteins stored in the ooplasm of GV stage-arrested oocytes drive oocyte meiosis and early embryonic development. Our study revealed a previously unreported function for RTCB in mouse oocyte maturation. RTCB conditional knockout mice exhibited a phenotype of female infertility, suggesting the important role of RTCB-mediated mRNA splicing in female fertility. The female infertility phenotype can be attributed to multiple factors.

In contrast, the lack of RTCB caused premature ovarian failure in female mice after 6 weeks of age, and we detected the apoptosis signal of granulosa cells on ovarian sections at this stage; however, the ovaries of 4-week-old $Rtcb^{oo−/−}$ mice still contained many primordial, primary, secondary and antral follicles. However, regardless of *in vivo* superovulation or *in vitro* culture, most GV

oocytes from 6-week-old RTCB knockout mice have difficulty resuming meiosis. This result was not unexpected because *Rtcb* deletion resulted in the accumulation of many IR-containing mRNAs in the GV stage, including DNA methylation (*Mbd1*, *Dnmt3b*) and DNA damage repair-related mRNA (*Rad50*). These results imply that RTCB may be involved in regulating follicle activation, except for the first wave. Combined with changes in the oocyte transcriptome, premature ovarian failure may be a secondary effect caused by the decline in transcripts enriched in protein transport and DNA damage repair pathways.

IR accumulation of these transcripts leads to changes in protein levels. RAD50 is crucial for DNA damage repair, and decreased RAD50 protein levels may lead to GVBD failure (Inagaki et al., 2016). MBD1 and DNMT3B are crucial for regulating DNA methylation (Hendrich and Bird, 1998; Nowialis et al., 2019). The decreased levels of related proteins result in a series of epigenetic changes that impair the developmental potential of the oocyte and embryo. Although the oocytes that resumed meiosis were able to extrude the polar body and had normal chromosome alignment and spindle assembly, most of the MII oocytes from *Rtcb*$^{\text{oo}-/-}$ mice had difficulty with fertilization and ZGA was suppressed. Defects occur during subsequent fertilization and early embryonic development. This result illustrates that RTCB may be dispensable for oocyte maturation after the resumption of meiosis. However, epigenetic changes could affect the developmental potential of oocytes, and the defects become evident at the zygote stage; therefore, the process of ZGA cannot be completed. GVBD failure, premature ovarian failure and ZGA defects caused by epigenetic changes in GV stage oocytes lead to infertility in female mice. These phenotypes also illustrate that RTCB-regulated IR splicing is important for female reproduction.

In addition, we investigated the differences between AS types after *Rtcb* deletion in oocytes. Surprisingly, many AS events were observed, including SEs. However, no relevant studies have examined the correlation between RTCB and exon skipping. GO enrichment analysis showed that the relevant transcripts were mainly enriched in the category of RNA processing, which differed from the transcripts found in IRFinder. These results indicate that RTCB may act through other mechanisms in oocytes.

Our study found that *Rtcb* deletion caused IR accumulation and significantly downregulated the global levels of these IR-containing transcripts. In addition, this has not yet been reported. Different mRNA degradation pathway may cause decreased levels of IR-containing transcripts, which may be because they cannot synthesize proteins and are degraded by nonsense-mediated mRNA decay, as the intron retention of these transcripts affects their open reading frame. However, the decrease in the levels of other IR-free transcripts remains unclear.

Knocking out the *Rtcb* gene in mature mouse B cells leads to structural defects within the endoplasmic reticulum and insufficient antibody secretion (Jurkin et al., 2014). However, our study found that *Rtcb* deletion in oocytes led to obstacles in the meiotic process, premature ovarian failure and loss of fertility. *Xbp1* mRNA was the only confirmed target mRNA of RTCB. The different phenotypes in germ cells show that *Rtcb* affects tRNA and Xbp1 mRNA, potentially has other substrates, such as *Rad50* and *Dnmt3b*, and has an impact on fertility.

Our study examined the role of *Rtcb* across the life of the oocyte and transition to embryo. IR-containing mRNAs are spliced appropriately through RTCB to synthesize proteins and perform their functions. This mechanism can regulate oocyte meiosis and the subsequent early embryonic development.

MATERIALS AND METHODS

Mice
Rtcb$^{fl/fl}$ mice were engineered as described previously (Li et al., 2021) and provided by Prof. Nai-Zheng Ding from the College of Life Science, Shandong Normal University, Jinan City, China. To construct oocyte-specific knockout *Rtcb* mice, *Rtcb*$^{fl/fl}$ mice were bred with the *Gdf9-Cre* mouse line to excise loxP-flanked exon 4, thus generating *Rtcb*-conditional-knockout mice.

All mice were bred under specific pathogen-free (SPF) conditions in a stable environment, including 50-70% humidity, 20-22°C, a 12/12 h light/dark cycle, and food and water provided *ad libitum*. All the mice had a C57BL/6J genetic background. The experimental procedures were approved by the Zhejiang University Institutional Animal Care and Research Committee (approval ZJU20210252 to H.-Y.F.) and mouse care and use were conducted following the relevant guidelines and regulations of Zhejiang University. The primers used for genotyping are listed in Table S4. The age, sex and size of each sample are shown in the related figure legends.

Oocyte culture
Three-week-old female mice were intraperitoneally primed with 5 IU of pregnant mare serum gonadotropin (PMSG) and fully grown oocytes were obtained in M2 medium (M7167; Sigma-Aldrich) 44 h later. These oocytes were cultured in mini-drops of M16 medium (M7292; Sigma-Aldrich) covered with mineral oil (M5310; Sigma-Aldrich) and then incubated at 37°C in a 5% CO_2 atmosphere.

Cell culture
HEK 293T cells were obtained from ATCC and were recently authenticated and tested for contamination. Cells were cultured in DMEM plus 10% fetal bovine serum and 1% penicillin-streptomycin solution at 37°C in a humidified 5% CO_2 incubator.

Superovulation and fertilization
Three-week-old female mice were injected with 5 IU PMSG. These mice were injected with 5 IU of human chorionic gonadotropin (hCG) 44 h later. After an additional 16 h, oocyte-cumulus complexes were separated from the oviducts. Individual oocytes were obtained via digestion with hyaluronidase (Sigma-Aldrich). To acquire early embryos, 12-week-old wild-type males were mated with female mice. Vaginal plugs indicate successful mating. Embryos were obtained from oviducts at the indicated time points after hCG injection.

Plasmid construction and *in vitro* transcription
Continuously activated CDK1 was constructed by mutating T14 and Y15 of human CDK1 to alanine and phenylalanine, respectively. The corresponding cDNA was then subcloned into a FLAG-tagged expression vector (pDEST). The expression vector was linearized with HindIII and the linearized RNA was transcribed *in vitro* using the SP6 mMESSAGE mMACHINE kit (Invitrogen, AM1450). Phenol/chloroform extraction and ethanol precipitation were performed for RNA extraction and purification, respectively. The transcribed RNAs were *in vitro* polyadenylated using a poly (A) tailing kit (AM1350; Invitrogen).

Microinjection of mRNAs
All microinjections were performed using an Eppendorf TransferMan NK2 micromanipulator. Fully grown oocytes were cultured in M2 medium containing 2 μM milrinone to suppress spontaneous GVBD. Approximately 5-10 pl of 500 μg/ml mRNA was microinjected into the cytoplasm of the oocytes. As a negative control, 5-10 pl of 500 μg/ml transcribed RNA from the empty vector (pDEST-FLAG) was microinjected into the control oocytes. The oocytes were cultured in M16 medium containing 2 μM milrinone at 37°C in a 5% CO_2 atmosphere.

Quantitative RT-PCR
Total RNA was extracted from oocytes using an RNeasy Mini Kit (QIAGEN) according to the manufacturer's instructions. Reverse transcription was performed using a Superscript RT kit (Bio-Rad).

11

Quantitative RT-PCR was conducted using Power SYBR Green PCR Master Mix (Applied Biosystems, Life Technologies) with an ABI 7500 Real-Time PCR system (Applied Biosystems). The primers used are listed in Table S4.

Immunofluorescence
Oocytes were fixed with 4% paraformaldehyde (PFA) for 30 min and permeabilized for 20 min with 0.3% Triton X-100 in PBS. Antibody staining was performed according to previously described protocols (Zhang et al., 2020). The antibodies used in these experiments are listed in Table S5. Imaging was performed using a Zeiss LSM710 confocal microscope. Quantitative analysis of the fluorescence signals was performed using the ImageJ software.

EU incorporation assay
Embryos were cultured in KSOM medium with 100 µM 5-ethynyl uridine (EU) for 2 h. Fixation, permeabilization and staining were performed using the Click-iT RNA Alexa Fluor 488 Imaging Kit (ThermoFisher, 48 C10329) according to the manufacturer's protocol. The embryos were imaged using a Zeiss LSM710 confocal microscope.

Detection of protein synthesis
Oocytes were incubated in M2 medium primed with 100 mM L-homopropargylglycine (HPG) for 1 h. These oocytes were then fixed for 30 min in 4% PFA. HPG signals were examined using a Click-iT HPG Alexa Fluor Protein Synthesis Assay Kit (Life Technologies). The mean HPG signal was measured and quantified using ImageJ software.

Histological analysis
Ovaries were harvested and fixed in formalin overnight, processed and embedded in paraffin wax, according to standard protocols. The ovaries were serially sectioned at 5 µm and stained with Hematoxylin and Eosin. IHC was performed according to standard protocols. All the antibodies and their related dilution factors are listed in Table S5.

Western blot analysis
Oocytes were lysed in a loading buffer containing β-mercaptoethanol and then heated at 95°C for 10 min. Immunoblotting and SDS-polyacrylamide gel electrophoresis were performed following standard procedures using the Mini-PROTEAN Tetra Cell System (BioRad). All the antibodies and their related dilution factors are listed in Table S5.

RNA-seq library preparation and data analysis
Fully grown GV oocytes were collected from 6-week-old wild-type and *Rtcb^{fl/fl};Gdf9-Cre* female mice after PMSG (10 fully grown GV oocytes per sample). Ten oocytes with equal amounts of ERCC were subjected to each RNA-seq library construction. Total RNA was extracted using the RNeasy micro kit (Qiagen) following the manufacturer's instructions after picking the cells into 350 µl of lysis buffer supplied in the RNeasy micro kit (Qiagen). Libraries were prepared using a NEBNext Ultra RNA Library Prep Kit (Illumina). The libraries were sequenced on an Illumina platform with 150 bp paired-end reads. We used a script to filter out low-quality reads, and the clean reads were mapped to the mouse genome mm10 with TopHat (version 2.0.6). Gene expression levels were calculated and normalized to FPKM using cuffquant and cuffnorm. In RNA-seq data normalization, sequencing reads were mapped to an ERCC reference to obtain the percentage of ERCC reads in total reads. Gene expression levels were then normalized by multiplying the raw FPKM values by a normalization factor (normalization factor=percentage of ERCC in wild-type oocytes/percentage of ERCC in the sample). FPKM and mRNA copy numbers represent gene expression levels. Only the expressed genes (FPKM>1 in at least one sample) were considered in all analyses. A two-tailed Student's *t*-test was used to generate statistically significant values.

IR change analysis
Intron retention (IR) was analyzed using IRFinder software. The IR ratio was calculated as the ratio of unspliced exon-intron junction reads to total junction reads (unspliced exon-intron and spliced exon-exon). The IR change was calculated from the IR ratio of knockout samples minus that of wild-type samples. According to IRFinder, only these transcripts (IR change>0.1) exhibited obvious IR accumulation in all the analyses. Changes in IR in genes are shown in Table S1, and the IR number of the filter is shown in Table S2.

Analysis of various AS events
Using replicate multivariate analysis of transcript splicing (rMATS) (Shen et al., 2014), we detected five different AS events, including SE, A5SS, A3SS, MXE and retained intron (RI) (Shen et al., 2014). Various AS events were considered only when FDR<0.05. AS events are listed in Table S3.

Statistical analysis
Results are presented as mean±standard error of the mean (s.e.m.). Most experiments comprised at least three independent samples and were repeated at least three times. The results for the two experimental groups were compared using two-tailed unpaired Student's *t*-tests. *$P<0.05$, **$P<0.01$, ***$P<0.001$. At $P<0.05$, results were considered statistically significant. n.s. indicates a non-significant result.

Data availability
RNA-seq data have been deposited in GEO under accession number GSE190681.

Peer review history
The peer review history is available online at https://journals.biologists.com/dev/lookup/doi/10.1242/dev.200497.reviewer-comments.pdf

References
Adhikari, D. and Liu, K. (2014). The regulation of maturation promoting factor during prophase I arrest and meiotic entry in mammalian oocytes. *Mol. Cell. Endocrinol.* **382**, 480-487. doi:10.1016/j.mce.2013.07.027

Boothby, T. C., Zipper, R. S., van der Weele, C. M. and Wolniak, S. M. (2013). Removal of retained introns regulates translation in the rapidly developing gametophyte of Marsilea vestita. *Dev. Cell* **24**, 517-529. doi:10.1016/j.devcel.2013.01.015

Braunschweig, U., Gueroussov, S., Plocik, A. M., Graveley, B. R. and Blencowe, B. J. (2013). Dynamic Integration of Splicing within Gene Regulatory Pathways. *Cell* **152**, 1252-1269. doi:10.1016/j.cell.2013.02.034

Braunschweig, U., Barbosa-Morais, N. L., Pan, Q., Nachman, E. N., Alipanahi, B., Gonatopoulos-Pournatzis, T., Frey, B., Irimia, M. and Blencowe, B. J. (2014). Widespread intron retention in mammals functionally tunes transcriptomes. *Genome Res.* **24**, 1774-1786. doi:10.1101/gr.177790.114

Chakravarty, A. K. and Shuman, S. (2012). The sequential 2′,3′-cyclic phosphodiesterase and 3′-phosphate/5′-OH ligation steps of the RtcB RNA splicing pathway are GTP-dependent. *Nucleic Acids Res.* **40**, 8558-8567. doi:10.1093/nar/gks558

Chakravarty, A. K., Subbotin, R., Chait, B. T. and Shuman, S. (2012). RNA ligase RtcB splices 3′-phosphate and 5′-OH ends via covalent RtcB-(histidinyl)-GMP

and polynucleotide-(3′)pp(5′)G intermediates. *Proc. Natl. Acad. Sci. USA* **109**, 6072-6077. doi:10.1073/pnas.1201207109

Chen, T. P., Tsujimoto, N. and Li, E. (2004). The PWWP domain of Dnmt3a and Dnmt3b is required for directing DNA methylation to the major satellite repeats at pericentric heterochromatin. *Mol. Cell. Biol.* **24**, 9048-9058. doi:10.1128/MCB.24. 20.9048-9058.2004

Darnell, J. E. (2013). Reflections on the history of pre-mRNA processing and highlights of current knowledge: a unified picture. *RNA* **19**, 443-460. doi:10.1261/ rna.038596.113

Desai, K. K. and Raines, R. T. (2012). tRNA Ligase Catalyzes the GTP-Dependent Ligation of RNA with 3′-Phosphate and 5′-Hydroxyl Termini. *Biochemistry-Us* **51**, 1333-1335. doi:10.1021/bi201921a

Desai, K. K., Bingman, C. A., Phillips, G. N., Jr and Raines, R. T. (2013). Structures of the noncanonical RNA ligase RtcB reveal the mechanism of histidine guanylylation. *Biochemistry* **52**, 2518-2525. doi:10.1021/bi4002375

Ding, F., Cui, P., Wang, Z. Y., Zhang, S. D., Ali, S. and Xiong, L. M. (2014). Genome-wide analysis of alternative splicing of pre-mRNA under salt stress in Arabidopsis. *BMC Genomics* **15**, 431. doi:10.1186/1471-2164-15-431

Do, D. V., Strauss, B., Cukuroglu, E., Macaulay, I., Wee, K. B., Hu, T. X., Igor, R. D. L. M., Lee, C., Harrison, A., Butler, R. et al. (2018). SRSF3 maintains transcriptome integrity in oocytes by regulation of alternative splicing and transposable elements. *Cell Discov.* **4**, 33. doi:10.1038/s41421-018-0032-3

Englert, M., Xia, S. L., Okada, C., Nakamura, A., Tanavde, V., Yao, M., Eom, S. H., Konigsberg, W. H., Soll, D. and Wang, J. M. (2012). Structural and mechanistic insights into guanylylation by RNA-splicing ligase RtcB joining RNA between 3′-terminal phosphate and 5′-OH. *Proc. Natl. Acad. Sci. USA* **109**, 15235-15240. doi:10.1073/pnas.1213795109

Guijo, M., Ceballos-Chávez, M., Gómez-Marín, E., Basurto-Cayuela, L. and Reyes, J. C. (2018). Expression of TDRD9 in a subset of lung carcinomas by CpG island hypomethylation protects from DNA damage. *Oncotarget* **9**, 9618-9631. doi:10.18632/oncotarget.22709

Heald, R. and McKeon, F. (1990). Mutations of phosphorylation sites in lamin A that prevent nuclear lamina disassembly in mitosis. *Cell* **61**, 579-589. doi:10.1016/ 0092-8674(90)90470-Y

Hendrich, B. and Bird, A. (1998). Identification and characterization of a family of mammalian methyl-CpG binding proteins. *Mol. Cell. Biol.* **18**, 6538-6547. doi:10. 1128/MCB.18.11.6538

Iijima, K., Ohara, M., Seki, R. and Tauchi, H. (2008). Dancing on damaged chromatin: functions of ATM and the RAD50/MRE11/NBS1 complex in cellular responses to DNA damage. *J. Radiat. Res.* **49**, 451-464. doi:10.1269/jrr.08065

Inagaki, A., Roset, R. and Petrini, J. H. J. (2016). Functions of the MRE11 complex in the development and maintenance of oocytes. *Chromosoma* **125**, 151-162. doi:10.1007/s00412-015-0535-8

Jones, K. T. (2011). Anaphase-promoting complex control in female mouse meiosis. *Results Probl. Cell Differ.* **53**, 343-363. doi:10.1007/978-3-642-19065-0_ 15

Jørgensen, H. F., Ben-Porath, I. and Bird, A. P. (2004). Mbd1 is recruited to both methylated and nonmethylated CpGs via distinct DNA binding domains. *Mol. Cell. Biol.* **24**, 3387-3395. doi:10.1128/MCB.24.8.3387-3395.2004

Jurkin, J., Henkel, T., Nielsen, A. F., Minnich, M., Popow, J., Kaufmann, T., Heindl, K., Hoffmann, T., Busslinger, M. and Martinez, J. (2014). The mammalian tRNA ligase complex mediates splicing of XBP1 mRNA and controls antibody secretion in plasma cells. *EMBO J.* **33**, 2922-2936. doi:10. 15252/embj.201490332

Kosmaczewski, S. G., Edwards, T. J., Han, S. M., Eckwahl, M. J., Meyer, B. I., Peach, S., Hesselberth, J. R., Wolin, S. L. and Hammarlund, M. (2014). The RtcB RNA ligase is an essential component of the metazoan unfolded protein response. *EMBO Rep.* **15**, 1278-1285. doi:10.15252/embr.201439531

Li, R., Song, X.-T., Guo, S.-W., Zhao, N., He, M., He, C.-Q. and Ding, N.-Z. (2021). YY1 and RTCB in mouse uterine decidualization and embryo implantation. *Reproduction* **162**, 461-472. doi:10.1530/REP-21-0281

Lincoln, A. J., Wickramasinghe, D., Stein, P., Schultz, R. M., Palko, M. E., De Miguel, M. P. D., Tessarollo, L. and Donovan, P. J. (2002). Cdc25b phosphatase is required for resumption of meiosis during oocyte maturation. *Nat. Genet.* **30**, 446-449. doi:10.1038/ng856

Lu, Y., Liang, F.-X. and Wang, X. (2014). A Synthetic Biology Approach Identifies the Mammalian UPR RNA Ligase RtcB. *Mol. Cell* **55**, 758-770. doi:10.1016/j. molcel.2014.06.032

Maughan, W. P. and Shuman, S. (2016). Distinct Contributions of Enzymic Functional Groups to the 2′,3′-Cyclic Phosphodiesterase, 3′-Phosphate Guanylylation, and 3′-ppG/5′-OH Ligation Steps of the Escherichia coli RtcB Nucleic Acid Splicing Pathway. *J. Bacteriol.* **198**, 1294-1304. doi:10.1128/JB. 00913-15

Middleton, R., Gao, D., Thomas, A., Singh, B., Au, A., Wong, J. J.-L., Bomane, A., Cosson, B., Eyras, E., Rasko, J. E. J. et al. (2017). IRFinder: assessing the impact of intron retention on mammalian gene expression. *Genome Biol.* **18**, 51. doi:10.1186/s13059-017-1184-4

Morgan, D. O. (1995). Principles of CDK regulation. *Nature* **374**, 131-134. doi:10. 1038/374131a0

Ner-Gaon, H., Halachmi, R., Savaldi-Goldstein, S., Rubin, E., Ophir, R. and Fluhr, R. (2004). Intron retention is a major phenomenon in alternative splicing in Arabidopsis. *Plant J.* **39**, 877-885. doi:10.1111/j.1365-313X.2004.02172.x

Nowialis, P., Lopusna, K., Opavska, J., Haney, S. L., Abraham, A., Sheng, P., Riva, A., Natarajan, A., Guryanova, O., Simpson, M. et al. (2019). Catalytically inactive Dnmt3b rescues mouse embryonic development by accessory and repressive functions. *Nat. Commun.* **10**, 4374. doi:10.1038/s41467-019-12355-7

Pangas, S. A. and Rajkovic, A. (2006). Transcriptional regulation of early oogenesis: in search of masters. *Hum. Reprod. Update* **12**, 65-76. doi:10.1093/ humupd/dmi033

Popow, J., Englert, M., Weitzer, S., Schleiffer, A., Mierzwa, B., Mechtler, K., Trowitzsch, S., Will, C. L., Lührmann, R., Söll, D. et al. (2011). HSPC117 is the essential subunit of a human tRNA splicing ligase complex. *Science* **331**, 760-764. doi:10.1126/science.1197847

Reddy, A. S. N., Marquez, Y., Kalyna, M. and Barta, A. (2013). Complexity of the alternative splicing landscape in plants. *Plant Cell* **25**, 3657-3683. doi:10.1105/ tpc.113.117523

Shalgi, R., Hurt, J. A., Lindquist, S. and Burge, C. B. (2014). Widespread inhibition of posttranscriptional splicing shapes the cellular transcriptome following heat shock. *Cell Rep.* **7**, 1362-1370. doi:10.1016/j.celrep.2014.04.044

Shen, S., Park, J. W., Lu, Z.-X., Lin, L., Henry, M. D., Wu, Y. N., Zhou, Q. and Xing, Y. (2014). rMATS: robust and flexible detection of differential alternative splicing from replicate RNA-Seq data. *Proc. Natl. Acad. Sci. USA* **111**, E5593-E5601. doi:10.1073/pnas.1419161111

Shinya, S., Kadokura, H., Imagawa, Y., Inoue, M., Yanagitani, K. and Kohno, K. (2011). Reconstitution and characterization of the unconventional splicing of XBP1u mRNA in vitro. *Nucleic Acids Res.* **39**, 5245-5254. doi:10.1093/nar/gkr132

Stamm, S., Ben-Ari, S., Rafalska, I., Tang, Y. S., Zhang, Z. Y., Toiber, D., Thanaraj, T. A. and Soreq, H. (2005). Function of alternative splicing. *Gene* **344**, 1-20. doi:10.1016/j.gene.2004.10.022

Sudakin, V., Chan, G. K. T. and Yen, T. J. (2001). Checkpoint inhibition of the APC/ C in HeLa cells is mediated by a complex of BUBR1, BUB3, CDC20, and MAD2. *J. Cell Biol.* **154**, 925-936. doi:10.1083/jcb.200102093

Syed, A. and Tainer, J. A. (2018). The MRE11-RAD50-NBS1 complex conducts the orchestration of damage signaling and outcomes to stress in DNA replication and repair. *Annu. Rev. Biochem.* **87**, 263-294. doi:10.1146/annurev-biochem-062917-012415

Tan, J.-H., Wang, H.-L., Sun, X.-S., Liu, Y., Sui, H.-S. and Zhang, J. (2009). Chromatin configurations in the germinal vesicle of mammalian oocytes. *Mol. Hum. Reprod.* **15**, 1-9. doi:10.1093/molehr/gan069

Tanaka, N. and Shuman, S. (2011). RtcB is the RNA ligase component of an Escherichia coli RNA repair operon. *J. Biol. Chem.* **286**, 7727-7731. doi:10.1074/ jbc.C111.219022

Tanaka, N., Chakravarty, A. K., Maughan, B. and Shuman, S. (2011a). Novel mechanism of RNA repair by RtcB via sequential 2′,3′-cyclic phosphodiesterase and 3′-Phosphate/5′-hydroxyl ligation reactions. *J. Biol. Chem.* **286**, 43134-43143. doi:10.1074/jbc.M111.302133

Tanaka, N., Meineke, B. and Shuman, S. (2011b). RtcB, a novel RNA ligase, can catalyze tRNA splicing and HAC1 mRNA splicing in vivo. *J. Biol. Chem.* **286**, 30253-30257. doi:10.1074/jbc.C111.274597

Wong, J. J.-L., Ritchie, W., Ebner, O. A., Selbach, M., Wong, J. W. H., Huang, Y., Gao, D., Pinello, N., Gonzalez, M., Baidya, K. et al. (2013). Orchestrated intron retention regulates normal granulocyte differentiation. *Cell* **154**, 583-595. doi:10. 1016/j.cell.2013.06.052

Wu, J. and Hopper, A. K. (2014). Healing for destruction: tRNA intron degradation in yeast is a two-step cytoplasmic process catalyzed by tRNA ligase Rlg1 and 5′-to-3′ exonuclease Xrn1. *Genes Dev.* **28**, 1556-1561. doi:10. 1101/gad.244673.114

Zhang, J., Zhang, Y.-L., Zhao, L.-W., Guo, J.-X., Yu, J.-L., Ji, S.-Y., Cao, L.-R., Zhang, S.-Y., Shen, L., Ou, X.-H. et al. (2019). Mammalian nucleolar protein DCAF13 is essential for ovarian follicle maintenance and oocyte growth by mediating rRNA processing. *Cell Death Differ.* **26**, 1251-1266. doi:10.1038/ s41418-018-0203-7

Zhang, J., Zhang, Y.-L., Zhao, L.-W., Pi, S.-B., Zhang, S.-Y., Tong, C. and Fan, H.-Y. (2020). The CRL4-DCAF13 ubiquitin E3 ligase supports oocyte meiotic resumption by targeting PTEN degradation. *Cell. Mol. Life Sci.* **77**, 2181-2197. doi:10.1007/s00018-019-03280-5

Zhang, J., Liu, W., Li, G., Xu, C., Nie, X., Qin, D., Wang, Q., Lu, X., Liu, J. and Li, L. (2022). BCAS2 is involved in alternative splicing and mouse oocyte development. *FASEB J.* **36**, e22128. doi:10.1096/fj.202101279R

AQ11

Summary: The important role of RNA terminal phosphate cyclase B-regulated non-canonical splicing in female reproduction and the mechanisms involved.